HHS Public Access

Author manuscript

J Biophotonics. Author manuscript; available in PMC 2019 September 16.

Published in final edited form as:

J Biophotonics. 2018 June ; 11(6): e201700278. doi:10.1002/jbio.201700278.

A frequency-domain non-contact photoacoustic microscope based on an adaptive interferometer

Deepu George[1], **Harriet Lloyd**[2], **Ronald H. Silverman**[2], **Parag V. Chitnis**[1,*]

[1]Department of Bioengineering, George Mason University, Fairfax, Virginia

[2]Edward S Harkness Eye Institute, Columbia University Medical Center, New York, New York

Abstract

A frequency-domain, non-contact approach to photoacoustic microscopy (PAM) that employs amplitude-modulated (0.1–1 MHz) laser for excitation (638-nm pump) in conjunction with a 2-wave mixing interferometer (532-nm probe) for non-contact detection of photoacoustic waves at the specimen surface is presented. A lock-in amplifier is employed to detect the photoacoustic signal. Illustrative images of tissue-mimicking phantoms, red-blood cells and retinal vasculature are presented. Single-frequency modulation of the pump beam directly provides an image that is equivalent to the 2-dimensional projection of the image volume. Targets located superficially produce phase modulations in the surface-reflected probe beam due to surface vibrations as well as direct intensity modulation in the backscattered probe light due to local changes in pressure and/or temperature. In comparison, the observed modulations in the probe beam due to targets located deeper in the specimen, for example, beyond the ballistic photon regime, predominantly consist of phase modulation.

Graphical Abstract

[*]**Correspondence**: Parag V. Chitnis, Department of Bioengineering, George Mason University, Fairfax, VA., pchitnis@gmu.edu.

AUTHOR BIOGRAPHIES

Please see Supporting Information online.

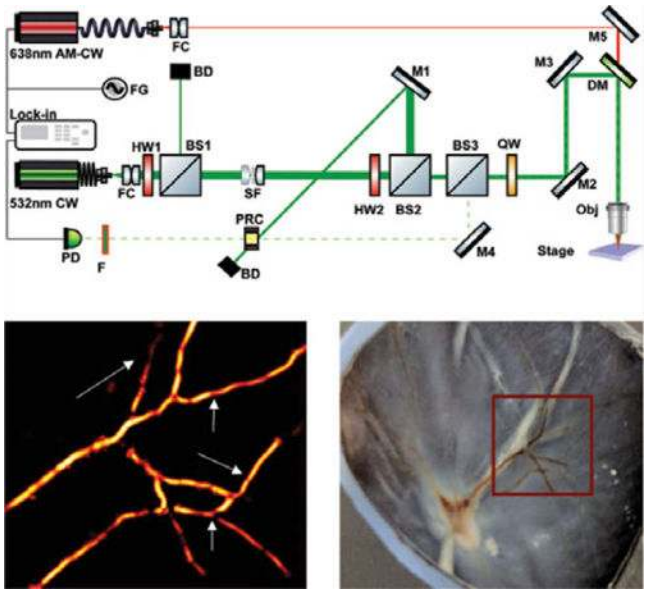

Keywords

interferometry; microscopy; photoacoustic imaging; photorefractive crystal

1 | INTRODUCTION

Photoacoustic microscopy (PAM) has found increasing medical and biological applications over the last couple of decades [1–5]. The technique relies on photoacoustic (PA) phenomenon, which refers to the absorption of monochromatic light and subsequent thermoelastic conversion of this energy into ultrasonic waves. Primary advantage lies in the fact that PAM combines molecular specificity of optics [3–6] with imaging depth and resolution associated with ultrasound. Therefore, PAM offers micron-resolution molecular imaging at depths (>1 mm) that are well beyond the limits of conventional optical techniques because (1) it does not require focused light and (2) in situ molecular information is relayed to the sensors acoustically, which is an (order of magnitude) less susceptible to scattering in tissue.

Most widely adopted PAM methods employ nanosecond or picosecond laser pulses to generate the PA signals and broadband ultrasound transducers to detect these signals. In acoustic-resolution PAM (AR-PAM) [6–8], diffuse optical radiation is used to generate the signals, while a focused transducer is used as the detector. Because signals are generated using diffused light, images can be obtained as deep as several millimeters. In AR-PAM, the spatial resolution, which is determined by the focusing properties of the ultra-sound transducer, typically ranges between 10 s of microns to a few hundred microns. In optical-resolution PAM (ORPAM) [9, 10], the excitation beam is focused to a micron or submicron spot and an unfocused transducer is used for detection. In this scheme, the lateral resolution is defined by the spot size of the excitation laser. But this scheme is limited to the ballistic-photon regime, which is typically limited to 1 mm or less [11]. In AR-PAM and OR-PAM,

the depth information is obtained by measuring the time of arrival of the PA pulses at the detector. The axial resolution, therefore, is limited by the bandwidth of the transducer.

The cost and size of high-energy pulsed lasers are among the factors limiting the proliferation and miniaturization of PAM systems. Laser jitter noise and attenuation of high frequencies in tissues also adversely affect the resolution. In direct acoustic detection, the transducer has to be kept in contact with the specimen using an appropriate coupling medium such as an ultrasound gel. For some applications such as surgical imaging or assessment of burn injuries, this requirement for transducer coupling is not desired [12, 13]. It is also a hindrance in ophthalmic imaging. Detection methods that require physical contact lead to patient discomfort. Further, physical motions of eye and head can affect the coupling. Transducer coupling also makes integration of PAM with other imaging modalities challenging [14].

The above issues have been addressed independently over the past several years. Frequency domain techniques in which the PA signals are generated by amplitude-modulated continuous-wave (CW) laser or sinusoidally driven laser diode has been proposed as an alternative to the pulsed excitation [15–18]. Many advantages offered by frequency domain techniques are discussed in the above references. CW lasers or diodes are cheaper and has smaller footprint and hence can aid in developing portable systems. When operating under the American National Standards Institute (ANSI)-prescribed safety limit, PA pressure generated with a sinusoidal excitation is about 6 orders of magnitude lower than that with pulsed excitation [19–21]. But for frequency domain imaging, the sensitivity can be enhanced using phase sensitive or lock-in detection. For a laser modulation of 100 MHz, this approach yields equivalent signal-to-noise ratio to that of pulsed excitation [17]. Depth-resolved imaging is not possible with single-frequency CW detection, but this can be achieved if frequency chirps are employed [20]. On the other hand, in several applications where region of interest lies in a thin layer, such as imaging of blood vessels in retina, depth-resolved imaging may not be necessary.

To alleviate the need for acoustical coupling, optical methods for detecting PA waves have been developed. Majority of these approaches rely on interferometric detection of the vibrations at the tissue surface resulting from the PA waves [12, 13, 22–27]. Surface displacements are encoded as phase modulations in an optical beam (signal beam) incident at the sample surface. These phase modulations are read out as intensity modulations obtained by interfering the signal beam with a reference beam. The amplitude of the modulations can be used to quantitatively determine the ultrasound amplitude [27, 28].

However, when coherent light is reflected off a rough surface, such as that in a biological specimen, the wavefront of the signal beam is distorted with speckles, each having a different optical phase than the rest. This leads to loss in sensitivity of the interferometer. This loss in sensitivity can be rectified using adaptive interferometers such as 2-wave mixing interferometers (TWMIs) [27, 29, 30]. In a TWMI with a photorefractive crystal (PRC), the reference and signal beams are brought to interfere inside the PRC, leading to the formation of a dynamic hologram due to the spatially non-uniform photoexcitation and the subsequent redistribution of charge carriers. Both the reference and signal beams are diffracted from this

hologram in the direction of the other with each of the diffracted beam's wavefront modified to match that of the non-diffracted beams [29]. The phase-matched signal beam and diffracted reference beam produce a high-contrast interference pattern on a photodetector (PD). The time of formation of hologram inside the crystal is determined by the response time of the PRC. Therefore, the PRC also acts as an optical high-pass filter. Low frequency noises from phase shifts slower than the response time are compensated by the reformation of the hologram, while high-frequency phase shifts between the beams lead to a change in intensity at the detector [30]. TWMI with PRC has been demonstrated to be well suited for the remote detection of PA signals from skin and tissue without the need of any coupling medium [12, 31]. The high-pass filter behavior of PRC is an added advantage when the system is implemented for in vivo imaging because it can potentially compensate for artifacts associated with bulk movements.

Despite possibilities for simplification of PA microscopes, attempts to combine frequency domain PAM (FdPAM) with non-contact optical detection have been scarce. In this paper, we present such a PA microscope, which uses an amplitude-modulated CW laser for PA generation and a PRC-based TWMI for detection. The microscope uses a coaxial scheme for excitation and detection, facilitating a simplified configuration. Furthermore, we demonstrate that FdPAM can directly provide an image that is equivalent to the 2-dimensional (2D) projection of a 3-dimensional (3D)–image volume.

2 | MATERIALS AND METHODS

2.1 | Two-wave mixing interferometer

A schematic diagram of the experimental setup is shown in Figure 1. Detection of PA waves is achieved using a 2-wave mixing adaptive interferometer that employs a PRC made of a 5 × 5 × 5 mm^3 $Bi_{12}SiO_{20}$ (BSO) crystal, cut along the [111] and [111] crystallographic axes. An electric field of 7 kV/cm is applied in the [1] direction in order to operate the crystal in the drift regime. A fiber-coupled CW laser with a wavelength of 532 nm (Excelsior FC, Spectra Physics, Santa Clara, CA) is used as the source for the interferometer. The output of the fiber laser is coupled into free space using a fiber optic collimator (TC18FC-543, Thorlabs Inc., Newton, NJ). A polarizing beam splitter (BS1) is used to select only the s-polarized (all polarizations mentioned in this manuscript are with respect to the plane of the table) beam. A half-wave plate (HW1) kept before the beam splitter enables the continuous adjustment of optical power of the beam delivered to the system. The beam is split into a p-polarized reference beam and an s-polarized signal beam using a second polarizing beam splitter (BS2). A second half-wave plate (HW2) placed before BS2 is used to select the power ratio between reference and signal beams. The reference beam is reflected off a mirror (M1) and directed toward the PRC. The signal beam passes through another polarizing beam splitter (BS3) and a quarter-wave plate (QW). As the signal beam is s-polarized, the beam passes through the beam splitter (BS3 was set to pass the s-polarization and reflect the p-polarization) in the forward direction. The fast axis of the quarter-wave plate is set to make an angle of 45° to the vertical direction. A periscopic assembly consisting of 3 mirrors, 2 dielectric (M2 and M3) and 1 dichroic (DM), directs the beam on to a long-working distance infinity-corrected microscope objective (10× or 100×), which

focuses the beam on the sample. The back reflected light from the sample is collected by the objective and collimated back into the beam path. After passing through the QW for a second time, the plane of polarization of the reflected signal beam is rotated by 90° with respect to its original polarization and thus becomes p-polarized. This back propagating signal beam gets reflected off PBS3 and is directed toward the PRC. The beam passes through the PRC onto a PD (HAS-XS-1G4-SI, Femto Messtechnik GmbH, Berlin, Germany). The reference beam and the signal beam interfere inside the PRC. The high-intensity reference beam is dumped into a beam dump (BD) after passing through the PRC.

2.2 | PA excitation

A fiber-coupled diode laser of wavelength 638 nm (iBeam SMART 640-S-FC, TOPTICA Photonics AG, Munich, Germany) is used to excite PA response. The excitation beam is collimated using a fiber collimator (F220APC-633, Thorlabs Inc., Newton, NJ). A function generator (3600A, Agilent, Santa Clara, CA) is used to modulate the intensity of the laser. The excitation laser is coupled into the final leg of the periscopic assembly through the dichroic mirror that passes 638 nm and reflects 532 nm. The sample is coaxially illuminated by the excitation and detection beam on the same spot using the objective eliminating the need for separate alignments for the 2 beams. A laser line filter (F) is placed in the return beam path to prevent any part of the excitation beam from reaching the PD.

2.3 | Image acquisition

Samples were placed on a 2D scanning system, consisting of 2 linear motorized stages (MTS50-Z8, Thorlabs Inc., Newton, NJ). The excitation beam was amplitude-modulated at a single frequency typically between 100 KHz and 1 MHz. All PA images shown in this manuscript were taken at 1 MHz laser modulation. Two-dimensional images were obtained by raster scanning the linear stages and recording the modulated probe signal, which was proportional to the amplitude of the PA wave produced at that location, using a lock-in amplifier (UHFLI, Zurich Instruments, Zurich, Switzerland) that provided 120 dB of dynamic reserve. Typical integration time used was 10 ms. Images were acquired using a 50-ms dwell time at each location.

When imaging tissue, the total optical intensity focused on the sample was adjusted to avoid photothermal damage. Laser spot size on the tissue surface was adjusted to be about 10 μm in diameter. The minimum probe beam power that gives a detectable signal at the PD was selected. For a tissue sample, this criterion resulted in a higher incident intensity for the probe beam because the reflection was typically less than 1%.

3 | RESULTS

3.1 | Sensitivity and resolution

The sensitivity of the TWMI was characterized by optically measuring the surface displacement of a pre-calibrated piezo electric transducer (TA0505D024, Thorlabs Inc., Newton, NJ) driven at its resonant frequency of 315 kHz. The transducer was driven using sinusoidal voltages with varying amplitudes from 5 V down to 10 mV. The transducer

displacement at voltages below 1 V were obtained by extrapolating manufacturer-specified calibration to this regime.

Figure 2A shows the magnitude of the lock-in signal as a function of transducer displacement. The inset of Figure 2A shows zoomed in plot for displacements up to 2 nm. The lowest applied voltage (10 mV), which was limited by the signal generator, corresponds to about 300 pm. By extrapolating this data to the noise floor of the system we estimate the minimum detectable surface displacement, u_{min}, for the interferometer as less than 100 pm.

In order to estimate the sensitivity of our system in terms of PA pressure values, we calculated the pressure (p) needed to generate the same surface displacements (u) in a typical tissue sample. The PA pressure is related to the surface displacements through the relation $p = Zu\pi f$ [12, 32], where Z is the impedance of the tissue (~$1{:}5 \times 10^6$ $^{Pa \cdot s}/_{m}$) and f the frequency of modulation. The transducer displacements in the above sensitivity measurements were converted to the equivalent expected pressure at the sample surface for a frequency of 1 MHz. Figure 2B shows the lock-in signal as a function of pressure up to 20 kPa. Following the same equation, the minimum detectable pressure, p_{min}, of the system was calculated as 470 Pa using u_{min} = 100 pm. As a reference, the initial pressure generated by absorption of optical energy for pulsed excitation is of the order of 10–20 kPa [1, 33]. Due to spherical expansion a 10-kPa pressure generated by an arbitrary spherical absorber will drop to roughly 1/10th of its amplitude when it reaches the tissue surface 6 Rs away, where Rs is the radius of the absorber [34]. As a rough estimate thus a 100 μm thick blood vessel, 500 μm below the surface should result in a surface displacement of 200 pm. It should be noted that if the laser exposure is kept the same, the pressure generated by CW excitation is expected to be several orders lower [20].

Within the ballistic-photon regime, the lateral-resolution in PAM is primarily determined by beam diameters of the detection and excitation beams. This resolution was characterized by scanning a high-frequency chromium NBS 1963A test target. Figure 3A shows the 2D image obtained from 10-μm lines. The resolution can be estimated alternatively by looking at the step response of the system when detecting an edge. Figure 3B shows normalized PA response from a single scan line across an edge taken with a scan step size of 2 μm. From the distance between the 90% and 10% points, the effective $1/e^2$ spot size or the resolution of our microscope can be estimated to be about 5.3 μm [35]. A higher resolution may be obtained by changing the microscope objective from 10× to 100×. It should be noted that this resolution is obtained for a surface absorber. For a real case scenario where the absorber is below the surface, the resolution will be degraded primarily due to the fact that OR-PAM techniques need to focus the laser inside the tissue. This is evident in the discussion of the hair phantom in the next section.

3.2 | Tissue-mimicking phantom

A multilayered phantom was constructed in order to determine the performance of the system in imaging samples with absorbers at different depths in a 3D volume. The sample consisted of 3 layers of hippocampus tissue each sliced to 500-μm thickness. Two pieces of hair strands ~80-μm thick were placed in between the layers. A 2D image of 1.5 mm^2 was

acquired and is shown in Figure 4. Because single-frequency modulation does not provide depth-resolved imaging, all the absorbers in the imaging volume are visible indiscriminately. However, the image correctly shows the hair strand in the vertical orientation at the top. There is only a slight variation in lateral resolution through the entire depth of the phantom as indicated by the relatively similar dimensions of the 2 hair strands in the image. This is because both the layers are still within the optical transport mean free path in tissues. The hair strand in the lower layer appears to be about 20% thicker than the one in the top layer. Thus a 2D image produced on this setup is equivalent to a 2D intensity projection of a 3D image taken using a time domain technique.

3.3 | Cell imaging

A PA image of red blood cells (RBCs) on a microscope slide, taken using a 100× objective is shown in Figure 5A. During the experiment a 10% saline solution was added to the top of the sample. After examining the microscope slide with an optical microscope, an area with a single layer of RBCs was selected to image using the PAM. The PA image shows a 50-μm^2 area. The step size used for scanning was 0.5 μm. A bright field optical microscope image of the same area is shown in Figure 5B for comparison. The characteristic biconcave shape associated with RBCs was successfully visualized by the PAM system. PAM visualized cells were approximately 8 μm in diameter, which was consistent with the dimensions determined from the bright-field image.

3.4 | Retinal microvasculature

Retinal layers were excised from porcine eyes and flat-mounted on glass microscope slides. A solution of 15% dextran was added to the top of the tissue to prevent sample dehydration. Figure 6A shows the PA images of a retinal sample. A photograph of the whole posterior hemisphere of the eye before transferring to the microscope slide is shown in Figure 6B. The area of which the PA image was scanned is marked with a red square. The PA image shows subsurface features which are not apparent in the photograph. Arrows in Figure 6A point to these subsurface features.

4 | DISCUSSION

4.1 | Incident power and safety considerations

ANSI establishes and publishes limits for “Safe Use of Lasers in Health Care Facilities.” For continuous exposure up to 10 s, the ANSI exposure limit for skin is $1.1{\cdot}10^4 \times (t)^{0.25}\mathrm{J/m^2}$ and the limit for point and source ocular exposure is $1.8{\cdot}10^1 \times (t)^{0.75}\mathrm{J/m^2}$, where t is the duration of exposure in seconds [36]. The corresponding maximum allowed intensities can be expressed as a function of exposure time as I_{skin}, $\mathrm{lim} = 1.1 \times 10^4 \times (t)^{-0.75}\mathrm{W/m^2}$ and I_{occu}, $\mathrm{lim} = 1.8 \times 10^1 \times (t)^{-0.25}\mathrm{W{=}m^2}$, respectively. For all the experiments in this manuscript, the optical power used for excitation was 1 mW and for probe was 10 mW. Thus, for a laser spot size of 10 μm in diameter, which was used for tissue imaging, and a dwell time of 50 ms, the exposure was 3 orders of magnitude higher than the safe limit for skin exposure. This was not a major concern for an ex vivo measurement, and no signs of thermal damage to the tissue sample were observed, but to adapt the technique for practical human applications, further optimizations will be required. For example, while imaging blood vessels, the spot

size can be expanded 5 times to 25 μm without a significant compromise in lateral resolution. Reducing the dwell time is another way to substantially reduce exposure. For tissue imaging, we used a dwell time (50 ms) which is 5 times the lock-in integration time (10 ms) to allow enough time for lock-in to settle to any change input. But it is conceivable to use a dwell time that is the same as the integration time [17]. In order to reduce the lock-in integration time, the laser modulation frequency needs to be increased significantly. The laser we used for PA generation was limited in modulation up to 1 MHz. But other authors have shown modulation up to 10 MHz using laser diodes and other lasers [17, 20]. Fast diode lasers capable of sinusoidal modulation of 100 MHz are already available. The CW laser power used for detection also needs to be addressed. Employing a laser in the infrared region as a detector would be an option. A TWMI based on GaAs PRC be an option in the infrared region. The minimum detectable pressure of 470 Pa which was estimated earlier is significantly higher than that of a typical Michelson type interferometer in which the minimum detectable displacement can be pushed down to low picometers. Hence, the overall sensitivity may increase with the adaptation of a Michelson interferometer despite the potential loss of sensitivity due to speckles.

4.2 | Physical mechanisms of probe-beam modulation

Optical detection of acoustic waves requires careful consideration because the reflected or backscattered optical (signal) beam may be modulated in several waves. Three mechanisms are generally discussed in literature in relation to PA detection: (1) photoacoustically induced surface vibrations can modulate the phase of the reflected optical beam, (2) subsurface changes in optical refractive index due to local changes in pressure can directly modulate the intensity of the backscattered probe beam [28, 37] and (3) subsurface changes in optical refractive index due to local changes in temperature (from light absorption) also can directly modulate the intensity of the backscattered probe beam [38, 39]. In addition to this, any low frequency thermal expansion or contraction of the absorber due to temperature change as a result of light absorption may also modulate the phase of the reflected beam from the interface. The first 2 mechanisms are a direct result of acoustic wave generation due to absorption of optical radiation, that is, PA effect, while the third and fourth are purely thermal effects. The third one is the basis of thermo-optical imaging. The detection mechanism described in this manuscript is mainly based on the first phenomenon, even though the thermo-optical technique has also been used to detect ultrasound [38, 39].

All 4 phenomena can play a role in our detection scheme to varying degrees depending on imaging depth and laser-modulation frequency. A prior study demonstrated that the magnitude of the PA signal generated using an amplitude-modulated laser is proportional to the modulation frequency, assuming 100% modulation depth of the laser [17]. Therefore, the modulations in the signal beam due to the first 2 mechanisms are expected to exhibit the same trend. However, the modulation depth of the excitation laser used in the present study deteriorated considerably once the modulation frequency exceeded 1 MHz. Therefore, we expect the signal generation from the PA mechanisms to peak around 1 MHz. On the other hand, thermo-optical signal will be more efficient at lower frequencies and would decrease as a function of increasing frequency. The lower cutoff frequency of the detection system in our case was determined by the photodiode and was around 10 KHz. Therefore, the thermo-

optical signal will be maximum at this frequency and should decrease with increasing frequency.

The depth of the absorber will also have varying impact on all the above described phenomena. When PA pressure waves are generated from absorbers located within the tissue medium, even at depths that exceed that of the ballistic-photon regime, the propagation of the PA wave and the subsequent phase modulation of the signal beam reflected from the surface are affected only by losses in magnitude associated with spherically spreading wave ($1/r$, where r is the depth of the absorber) and the frequency-dependent ultrasonic attenuation in tissue medium. On the other hand, because the mechanisms associated with local change in index of refraction are dependent on subsurface backscatter of the signal beam from the absorber location, contributions from these phenomena are also effected by attenuation of the optical beam employed for detection in the tissue medium. Therefore, these mechanisms will only contribute to the detected modulation signal when the absorbers located superficially, typically in the depths corresponding to the OR-PAM range, similar to an optical microscope with absorption contrast [40, 41].

A recent study on non-interferometric non-contact PAM [37] used modulation in a reflected low coherence probe beam as the detection method. It should be pointed out that the physical mechanism here is the same as the refractive index modulation due to acoustic pressure described above. Apart from being a non-interferometric method, the key difference in that study is that the detection is at the site of the absorption, whereas here we detect surface vibrations due to acoustic waves propagating to the surface. A detection in the vicinity of the absorber requires the backscattered beam to be collected from a depth, potentially decreasing the depth of imaging but at the same time avoids acoustic degradation of higher frequencies, which is typical for surface detection. Also, while a non-interferometric method avoids typical interference artifacts, here we overcome that with a TWMI.

The phase modulations resulting from the first mechanism are converted into corresponding intensity modulations by the interference of the signal and reference beams inside the PRC as well as at the photodiode. Blocking the reference beam will eliminate contribution of phase modulation allowing one to observe only the intensity modulations resulting from any local changes in the refractive index. But we note that the reverse may not be true, that is, pure intensity modulations in the signal beam may also contribute to the interferometric signals due to change in the intensity of the signal beam. In that sense, when a reference beam is present, it may not be possible to separate out the contribution from thermal effects to the overall signal without additional considerations of depth, frequency and so on.

Based on the above considerations, we hypothesized that for absorbers at or near the surface, a detection mechanism mediated by the refractive index modulation will be the most prominent. But as the depth of the absorber increases, the efficiency of this modulation will rapidly decrease and the phase modulation due to surface vibrations will be more effective. To test this hypothesis, we recorded the signals from the lock-in amplifier for 2 different absorbers—one at the surface and one 1 mm below (past the ballistic-photon regime) the surface. Both signals were recorded for a range of modulation frequencies. Figure 7A shows

the detected lock-in signals for the surface absorber, while Figure 7B shows the signal from the subsurface absorber. The surface absorber shows a rapid drop in signal as a function of increasing modulation frequency with a smaller peak at 1 MHz. The detected signal at lower frequencies is dominated by the thermo-optic effect, while the peak at 1 MHz corresponds to the frequency at which our excitation laser most efficiently generates PA waves. For the absorber below the surface, the trend is reversed because the dominant contribution to the observed signal comes from the PA waves that propagate to the surface and produce surface vibrations and subsequent phase modulation. Dashed lines in both figures shows the lock-in signal when the reference beam is blocked. The high-frequency response is mostly eliminated when the reference is blocked. At the low end of frequency, modulation is present even without the reference beam, even though presence of the reference amplifies the signal. The amplification may be due to 2 factors: (1) the low-frequency signal may not be a pure intensity modulation that points to possible thermal expansion and contraction and (2) intensity modulation in the signal beam gets amplified by the interferometer.

5 | CONCLUSIONS

In this paper, we introduced a frequency-domain non-contact PA microscope utilizing solid state CW lasers for excitation and detection of acoustic signal. PA signals of phantoms and ex vivo samples were measured with a lock-in amplifier. As the microscope operates at a single-frequency excitation, the resulting images are 2D projection of 3D structures in the sample. The modulation frequency was limited to 1 MHz due to the constraints associated with the excitation laser. We also examined the different possible mechanisms that contribute to the signal and explored the effect of frequency and depth on each. Using a laser capable of modulating at higher frequencies will increase the PA-pressure magnitude and potentially increase the sensitivity of the system, which will in turn facilitate operation of such microscope systems under the ANSI safety limits.

ACKNOWLEDGMENTS

The authors acknowledge funding from the National Eye Institute at the National Institutes of Health (1R21EY023012).

Funding information

National Eye Institute, Grant/Award number: 1R21EY023012

REFERENCES

[1]. Changhui L, Lihong VW, Phys. Med. Biol 2009, 54, R59. [PubMed: 19724102]

[2]. Yao J, Wang LV, Laser Photonics Rev. 2013, 7, 758 10.1002/lpor.201200060.

[3]. Xu M, Wang LV, Rev. Sci. Instrum 2006, 77, 041101.

[4]. Wang X, Xie X, Ku G, Wang LV, Stoica G, J. Biomed. Opt 2006, 11, 024015. [PubMed: 16674205]

[5]. Grinvald A, Lieke E, Frostig RD, Gilbert CD, Wiesel TN, Nature 1986, 324, 361. [PubMed: 3785405]

[6]. Zhang HF, Maslov K, Stoica G, Wang LV, Nat. Biotechnol 2006, 24, 848. [PubMed: 16823374]

[7]. Cai D, Li Z, Chen S-L, Biomed. Opt. Express 2016, 7, 369. [PubMed: 26977346]

[8]. Cai D, Li Z, Li Y, Guo Z, Chen S-L, Opt. Express 2017, 25, 1421. [PubMed: 28158024]

[9]. Hu S, Wang LV, Biophys. J 2013, 105, 841. [PubMed: 23972836]
[10]. Maslov K, Zhang HF, Hu S, Wang LV, Opt. Lett 2008, 33, 929. [PubMed: 18451942]
[11]. Hu S, Maslov K, Wang LV, Opt. Lett 2011, 36, 1134. [PubMed: 21479007]
[12]. Hochreiner A, Bauer-Marschallinger J, Burgholzer P, Jakoby B, Berer T, Biomed. Opt. Express 2013, 4, 2322. [PubMed: 24298397]
[13]. Rousseau G, Gauthier B, Blouin A, Monchalin J-P, J. Biomed. Opt 2012, 17, 0612171.
[14]. Liu W, Zhang HF, Photoacoustics 2016, 4, 112. [PubMed: 27761410]
[15]. Maslov K, Wang LV, J. Biomed. Opt 2008, 13, 024006. [PubMed: 18465969]
[16]. Telenkov S, Mandelis A, Lashkari B, Forcht M, J. Appl. Phys 2009, 105, 102029.
[17]. Langer G, Buchegger B, Jacak J, Klar TA, Berer T, Biomed. Opt. Express 2016, 7, 2692. [PubMed: 27446698]
[18]. Mohajerani P, Kellnberger S, Ntziachristos V, Photoacoustics 2014, 2, 111. [PubMed: 25431755]
[19]. Petschke A, La Rivière PJ, Biomed. Opt. Express 2010, 1, 1188. [PubMed: 21258540]
[20]. Maslov KI, Wang LV, J. Biomed. Opt 2008, 13(2), 024006. [PubMed: 18465969]
[21]. Yao J, Wang LV, Photoacoustics 2014, 2, 87. [PubMed: 25302158]
[22]. Murray TW, Balogun O, Appl. Phys. Lett 2004, 85, 2974.
[23]. Wang Y, Li C, Wang RK, Opt. Lett 2011, 36, 3975. [PubMed: 22002357]
[24]. Hochreiner A, Reitinger B, Bouchal KD, Zamiri S, Burgholzer P, Berer T, J. Mod. Opt 2013, 60, 1327. [PubMed: 24347820]
[25]. Ing RK, Monchalin JP, Appl. Phys. Lett 1991, 59, 3233.
[26]. Tian C, Feng T, Wang C, Liu S, Cheng Q, Oliver DE, Wang X, Xu G, IEEE Sens. J 2016, 16, 8381. [PubMed: 28210188]
[27]. Berer T, Hochreiner A, Zamiri S, Burgholzer P, Opt. Lett 2010, 35, 4151. [PubMed: 21165120]
[28]. Dong B, Sun C, Zhang HF, IEEE Trans. Biomed. Eng 2017, 64, 4. [PubMed: 27608445]
[29]. Kamshilin AA, Romashko RV, Kulchin YN, J. Appl. Phys 2009, 105, 031101.
[30]. Tokuyuki H, Toshihisa Y, Hirokazu M, Jpn. J. Appl. Phys 1995, 34, 3737.
[31]. Hochreiner A, Berer T, Grun H, Leitner M, Burgholzer P, Biophotonics J 2012, 5, 508.
[32]. Rousseau G, Blouin A, Monchalin JP, Biomed. Opt. Express 2012, 3, 16. [PubMed: 22254164]
[33]. Beard P, Interface Focus 2011, 1, 602. [PubMed: 22866233]
[34]. Wang LV, IEEE J. Sel. Top. Quantum Electron. 2008, 14, 171.
[35]. Siegman AE, Sasnett MW, Johnston TF, IEEE J. Quantum Electron. 1991, 27, 1098.
[36]. American National Standards Institute, American National Standard for the Safe Use of Lasers in Healthcare Facilities: Standard Z136.1–2014, ANSI Inc., New York 2014.
[37]. Hajireza P, Shi W, Bell K, Paproski RJ, Zemp RJ, Light Sci. Appl 2017, 6, e16278. [PubMed: 30167263]
[38]. Paltauf G, Schmidt-Kloiber H, Guss H, Appl. Phys. Lett 1996, 69, 1526.
[39]. Paltauf G, Schmidt-Kloiber H, Köstli KP, Frenz M, Appl. Phys. Lett 1999, 75, 1048.
[40]. Lukkala M, Penttinen A, Electron. Lett 1979, 15, 2.
[41]. Rosencwaig A, Busse G, Appl. Phys. Lett 1980, 36, 725.

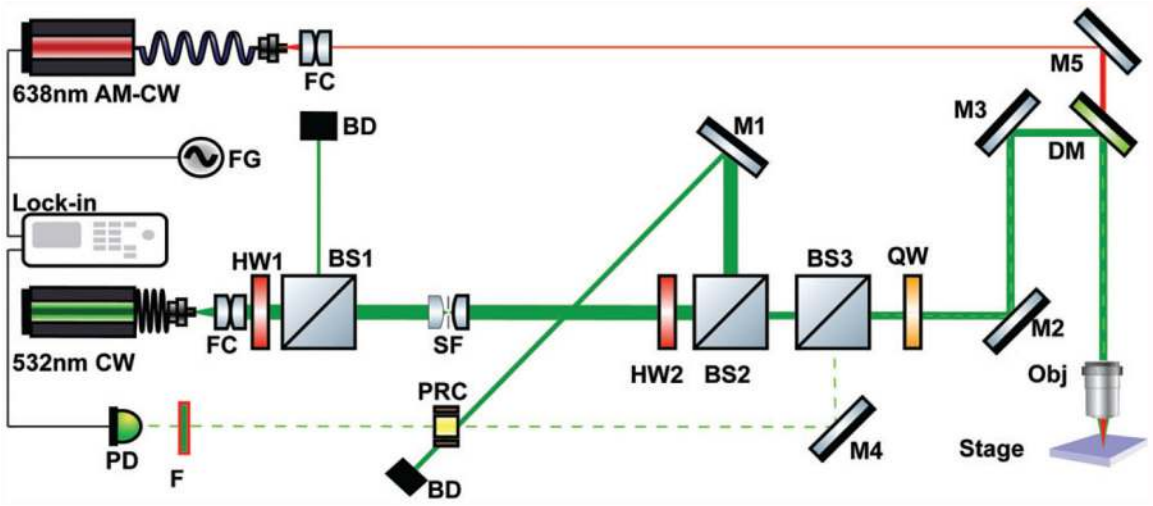

FIGURE 1.
Schematic of the PRC-based PAM system

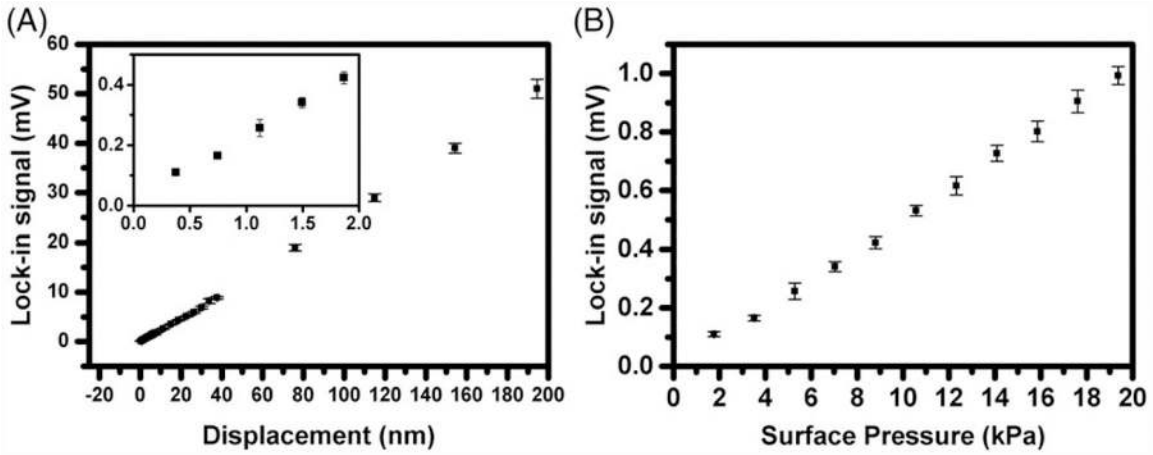

FIGURE 2.

Signal from the lock-in amplifier as a function of surface displacement (A) and calculated equivalent pressure (B)

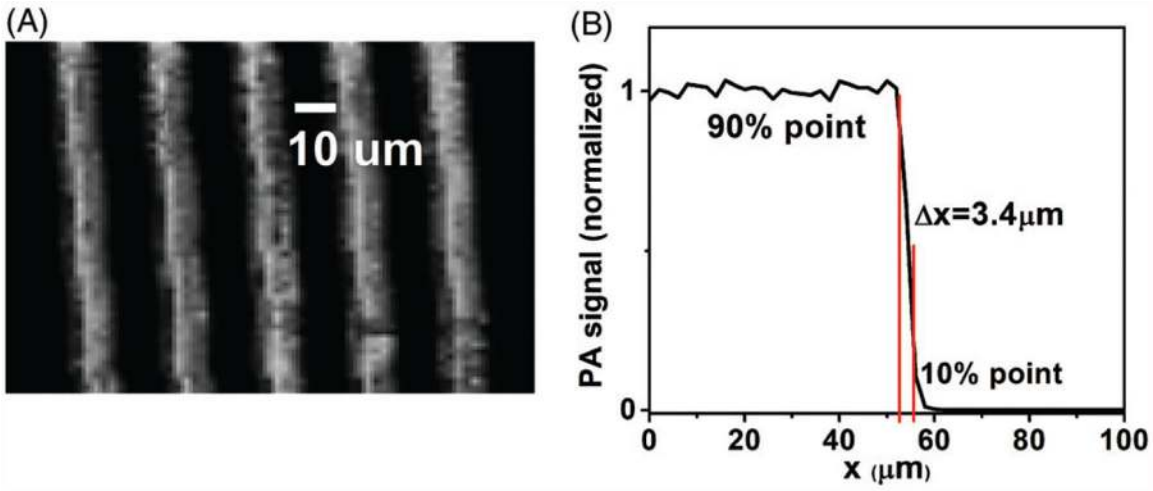

FIGURE 3.
(A) Photoacoustic image of chrome target; (B) PA image of an edge of thick chrome line

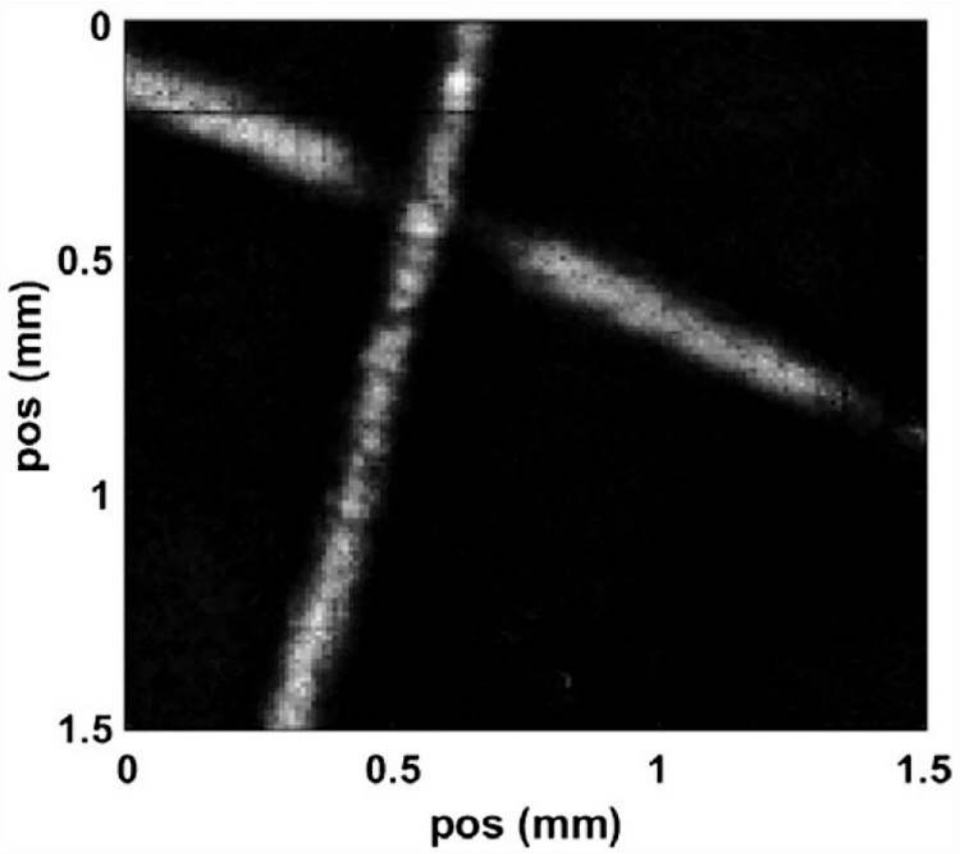

FIGURE 4.
Photoacoustic image of human hair embedded in multiple layers of hippocampus tissue

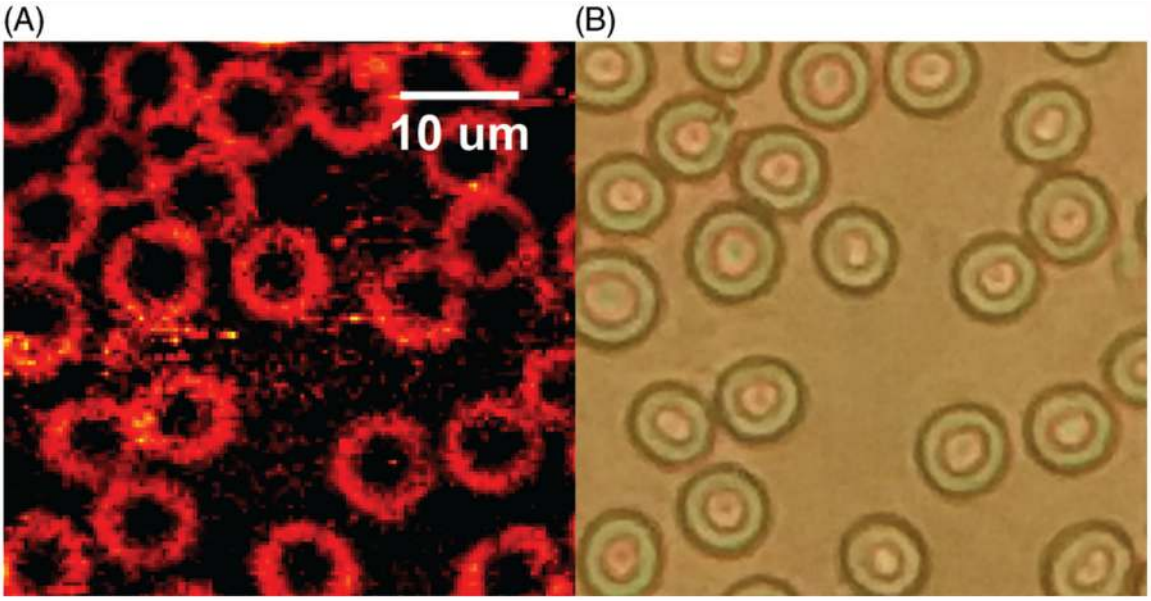

FIGURE 5.
(A) PA image of blood smear showing RBC; (B) corresponding bright field image

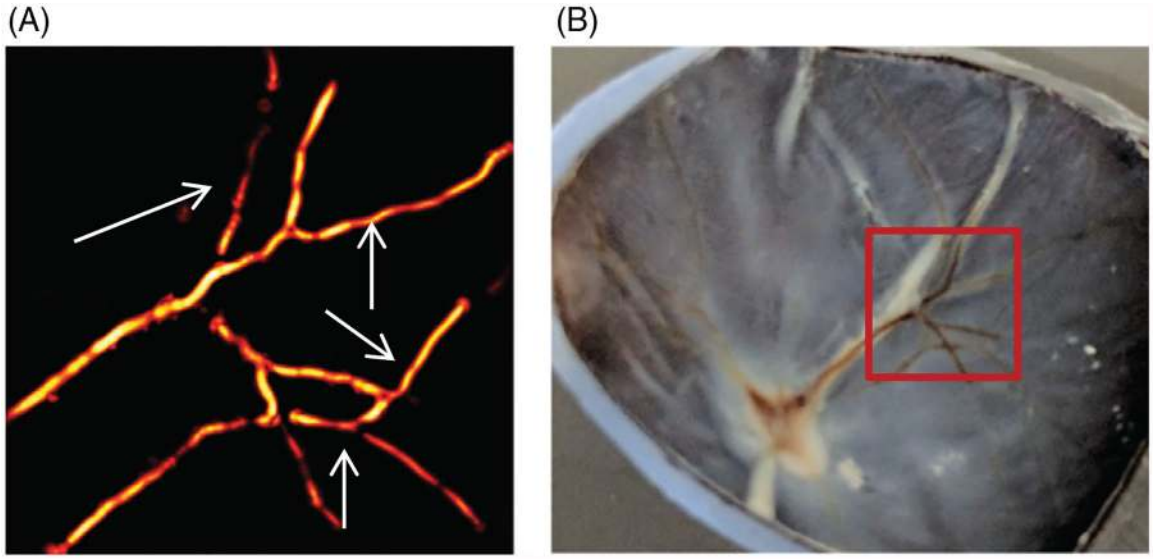

FIGURE 6.
(A) PAM image of ex vivo retinal samples. (B) Photograph of the sample

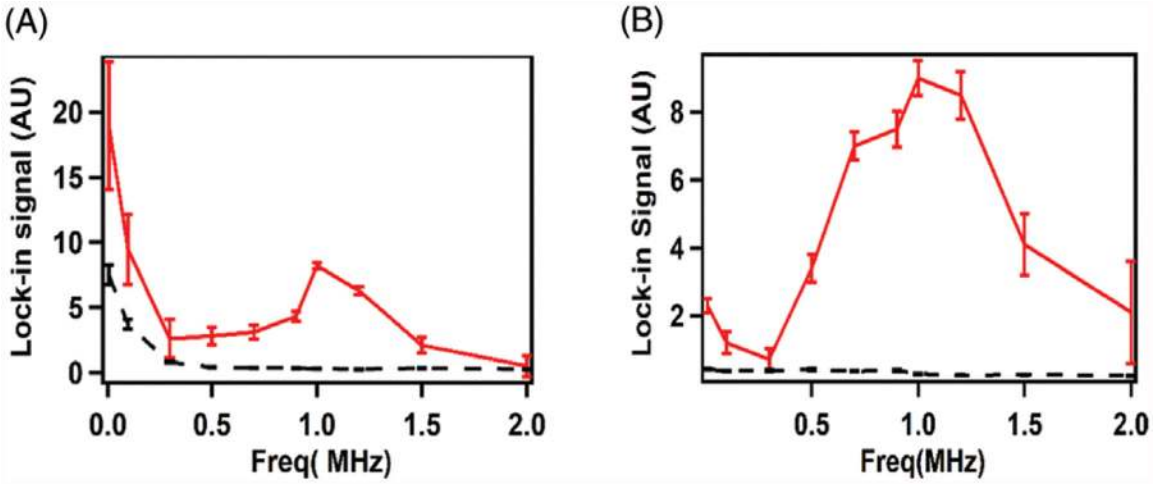

FIGURE 7.

(A) Signal detected by the lock-in as a function of frequency for an absorber at the surface. (B) Signal for an absorber at depth 1 mm . Dashed lines show the signal without the reference beam